



**HAL**  
open science

# **Influence of the lateral confinement on the transverse mechanical behavior of tows and quasi-unidirectional fabrics: Experimental and modeling investigations of dry through-thickness compaction**

Julie Hemmer, Anne-Sophie Lectez, Erwan Verron, Jean-Michel Lebrun,  
Christophe Binetruy, Sébastien Comas-Cardona

## ► To cite this version:

Julie Hemmer, Anne-Sophie Lectez, Erwan Verron, Jean-Michel Lebrun, Christophe Binetruy, et al.. Influence of the lateral confinement on the transverse mechanical behavior of tows and quasi-unidirectional fabrics: Experimental and modeling investigations of dry through-thickness compaction. *Journal of Composite Materials*, 2020, 54 (23), pp.3261-3274. 10.1177/0021998320912809. hal-04586134

**HAL Id: hal-04586134**

**<https://hal.science/hal-04586134>**

Submitted on 27 May 2024

**HAL** is a multi-disciplinary open access archive for the deposit and dissemination of scientific research documents, whether they are published or not. The documents may come from teaching and research institutions in France or abroad, or from public or private research centers.

L'archive ouverte pluridisciplinaire **HAL**, est destinée au dépôt et à la diffusion de documents scientifiques de niveau recherche, publiés ou non, émanant des établissements d'enseignement et de recherche français ou étrangers, des laboratoires publics ou privés.

# Influence of the lateral confinement on the transverse mechanical behavior of tows and quasi-unidirectional fabrics: Experimental and modeling investigations of dry through-thickness compaction

Julie Hemmer<sup>1</sup>, Anne-Sophie Lectez<sup>1,2</sup>, Erwan Verron<sup>1</sup>, Jean-Michel Lebrun<sup>1</sup>,  
Christophe Binetruy<sup>1</sup> and Sébastien Comas-Cardona<sup>1</sup>

Fibrous textiles are subjected to dry through-thickness compaction during most of the composites manufacturing processes. Usual tow models implemented in textile numerical simulations do not reproduce the tow widening occurring during the compaction. Nonetheless, this widening (that can reach 10%) would influence the internal microstructure of the considered fabric and its mechanical behavior. This paper proposes a simple mechanical approach to reproduce the width and thickness evolutions experimentally measured during through-thickness compaction of E-glass and carbon tows. Once the material parameters identified on laterally free tows, the tow cross-section model is employed to study the influence of the tow lateral confinement on the transverse mechanical behavior of its corresponding quasi-unidirectional fabric. It is observed that the lateral confinement depends on the quasi-unidirectional stitch tension. This confinement induces a densification of the tows leading to a stiffening of the quasi-unidirectional transverse behavior. This stiffening is well predicted by the proposed modeling approach.

Keywords: Mechanical analysis, analytical modeling, fiber tow, fabrics/textiles, transverse compression

## Introduction and previous work

During dry composite manufacturing processes (RTM, C-RTM, infusion), the fibrous material is impregnated by a liquid resin after being compacted during mold closing or vacuum setting. This through-thickness compaction of dry fabrics has been extensively studied over the last decades at macroscopic scale: experimental characterizations have been conducted on woven fabrics,<sup>1-4</sup> quasi unidirectional non-crimp fabrics (NCF; quasi-UD NCF)<sup>5,6</sup> or mats<sup>7</sup> and models have been developed to predict the fiber volume fraction  $V_f$  and the stack thickness evolutions with the applied pressure.<sup>8-11</sup> When quasi-UD or woven fabrics are considered for structural applications, the microstructure i.e. tows size and spatial distribution within the fabric, is of primary interest as it impacts the pore size and tortuosity and thus the overall in-plane and out-of-plane

fabric permeabilities,<sup>12-15</sup> as well as the mechanical properties of the final composite part (failure initiation<sup>16</sup> and crack propagation).

It fueled the interest in predicting the textile mechanical behavior during compaction from the initial textile architecture and the tow mechanical behavior. The textile architecture is numerically generated either from a software (TexGen<sup>17,18</sup>), a 3D image<sup>19,20</sup> or from geometrical considerations.<sup>11</sup> Constitutive tows can be either viewed as a continuum material or as a collection

---

<sup>1</sup>GeM Institute, UMR CNRS 6183, France

<sup>2</sup>Centre National d'Études Spatiales (CNES), France

### Corresponding author:

Julie Hemmer, GeM Institute, UMR CNRS 6183, Ecole Centrale de Nantes, 1 rue de la Noe, 44321, Nantes Cedex 3, France.  
Email: julie.hemmer@ec-nantes.fr

of fibers. For a continuum formulation, classical solid mechanics can be applied and most models are derived in the framework of hypoelasticity<sup>17</sup> and hyperelasticity,<sup>21</sup> or empirically fitted, for example with power law functions.<sup>22</sup> If tows are described as a collection of fibers, most models are based on fiber distances<sup>23</sup> or fiber-fiber friction.<sup>24</sup>

To the author's knowledge, the multi-chain digital element model (based on fiber-fiber friction) proposed by Zhou et al.<sup>24</sup> is the only one that predicts the tows widening occurring during through-thickness compaction.<sup>25</sup> However, this tow widening can experimentally reach 10%<sup>23,26</sup> and has been observed during both single tow compaction<sup>18,23,26</sup> and plain woven fabric compaction.<sup>25</sup> It is therefore of interest to provide a simple mechanical model that predicts both the width and thickness change experienced by tows during through-thickness compaction.

Additionally, the internal microstructure and transverse mechanical behavior of fabrics are affected by tow widening, as highlighted by Vallons et al.<sup>6</sup> who studied the influence of the stitching pattern on the microstructure and the transverse mechanical behavior of E-glass NCFs. The quasi-UD stitch pattern seems to modify locally the lateral confinement of its constitutive tows and thus the overall fabric transverse mechanical behavior. Therefore, it is of great interest to propose a first investigation of the constitutive tow lateral confinement influence on the mechanical response of quasi-UDs subjected to through-thickness compaction.

## Objectives and content of the study

The main objectives of the study are threefold:

- quantify the width and thickness evolutions of dry single tows and quasi-UDs during through-thickness compaction,
- propose a 2D continuum mechanical model that reproduces both the lateral and the transverse behaviors of E-glass and carbon tows,
- predict a transverse mechanical behavior range for quasi-UDs based on the transverse behavior of their respective tows and their lateral confinement.

Experiments are conducted to monitor both the width and the thickness evolutions of E-glass and carbon tows and their corresponding quasi-UDs when subjected to through-thickness compaction. The designed setup and developed post-processing methods are first pointed out and experimental results are discussed. Then, a simple continuum mechanical approach is proposed to reproduce the lateral and transverse evolutions of tows. Two lateral boundary conditions (free edge condition that allows tow widening and confined

edge condition that prevents tows from widening) are considered and expressed analytically. The material parameters of the obtained 2D constitutive model are selected to best fit the experimental behavior of laterally free carbon and E-glass tows. Finally, a novel comparison is proposed between the predicted behavior of laterally confined carbon and E-glass tows on one side and the experimental behavior of carbon and E-glass quasi-UDs on the other side.

## Materials of the study

### Fabrics

One carbon quasi-unidirectional woven fabric and two E-glass quasi-UD NCF have been selected for the study. The highly unbalanced carbon quasi-UD (named UD-C) provided by Chomarat has a total areal weight of 687 g/m<sup>2</sup> and is made of warp carbon tows (50 k fibers per tow) and weft E-glass tows, spaced at intervals of 8 mm. The two E-glass quasi-UD NCFs provided by Owens Corning have both a total E-glass areal weight of 1395 g/m<sup>2</sup> and are made of two layers: one warp layer of UD E-glass tows (4800 tex) and one weft backing E-glass layer oriented at  $\pm 80^\circ$  (68 tex). Both layers are stitched (warp-knitting) with a PET yarn whose mass is negligible. The only difference between the two E-glass NCFs is the stitch pattern: the first NCF (named UD-tight) has a symmetrical stitch pattern with a 2.5 mm stitch spacing whereas the stitch patterns of the second NCF (named UD-loose) is asymmetrical, 5 mm spaced and looser.

### Tows

Experiments are conducted on carbon tows extracted from UD-C, E-glass tows extracted from UD-loose, and E-glass tows extracted from UD-tight. No binders were added to the extracted tows. The characteristics of fabrics and their corresponding tows are reported in Table 1.

## Experimental setup and methods

The specific setup and experimental protocol developed to quantify the width and thickness evolutions of fibrous samples during compaction are presented hereafter. Mechanical variables (extensions and stress) are also defined to compare the results obtained on carbon and E-glass tows and quasi-UDs.

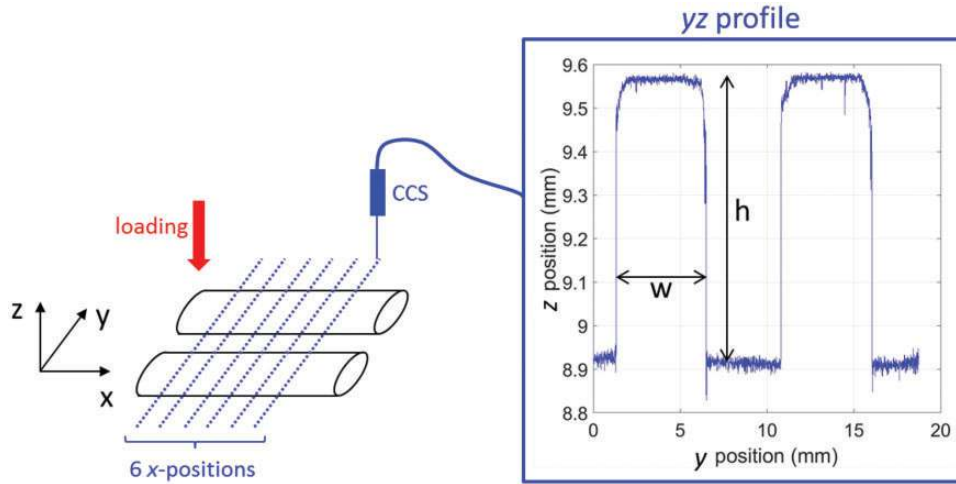
### Setup

A compression device has been specially designed to apply uniaxial transverse compression ( $z$ -direction) on

**Table 1.** Specifications of the studied fibrous materials (fabrics and tows).

Material name	Fiber		Tow		Fabric		
	Nature		Number of fibers per tow	Lineal weight (g/m)	Areal weight (gm <sup>2</sup> )	Stitch spacing (mm)	Weft spacing (mm)
UD-C	HS carbon		50,000	3.8	687	–	8
UD-tight	E-glass		8000	4.8	1395	2.5–symmetrical	–
UD-loose	E-glass		8000	4.8	1395	5–asymmetrical	–

UD: unidirectional; UD-C: carbon quasi-unidirectional.

**Figure 1.** Measurement principle with the CCS and typical data obtained ( $yz$  profiles, thickness  $h$  and width  $w$ ) with tows at a given  $x$ -position and force level.

CCS: chromatic confocal scanner.

tows or fabrics under a chromatic confocal scanner (CCS), which measures the width and thickness of the fibrous sample (Figure 1). It is composed of a micro-metric compact lab jack through which vertical displacements ( $z$ -direction) are applied, a 2 kN cell force, a bottom mobile steel platen, and a top PMMA plate, bonded to a steel frame. Calibration of this setup and more details are presented by Dharmalingam et al.<sup>26</sup>

### Experimental protocol

The compression device is mounted on the moving support of the CCS and the fibrous sample is placed on the bottom mobile steel platen. It is assumed that the friction between the fibrous sample and the experimental device (PMMA and steel plates) is negligible compared to the friction occurring between the fibers inside the considered sample. Fibrous sample altitude profiles ( $yz$ ) are measured through the PMMA plate at several  $x$ -positions with an optical pen (linked to the CCS light controller via optical fiber, see CCS Prima STIL for details) whose specifications are given in Table 2.

**Table 2.** Specifications of the optical pen used to acquire  $yz$  profiles of tows and quasi-UDs.

Optical pen reference	CL4
$xy$ resolution	7 $\mu\text{m}$
Thickness ( $z$ ) range	4000 $\mu\text{m}$
Thickness ( $z$ ) accuracy	0.200 $\mu\text{m}$

The thickness of the cavity is gradually reduced to apply a force on the fibrous sample going from 2 to 80 N. The measured force stabilizes after 2 min due to fiber relaxation. For each force level, 6  $yz$  profiles are recorded. For each  $yz$  profile, a  $z$ -position is measured every 5  $\mu\text{m}$  in the  $y$ -direction, allowing the determination of both the sample width ( $w$ ) and thickness ( $h$ ) (Figure 1) with good accuracy.

Tests have been carried out on tows and fabrics according to this experimental protocol. No additional tensile force along the  $x$ -axis has been added to the ends of the considered fibrous sample. For tow tests, 2 tows of 70 mm length are laid down on the cavity. For fabric

tests, a sample composed of 3 tows of 46.5 mm length is placed on the platen and tape is added at the lateral edges ( $x$ -direction, as highlighted in Figure 2) to maintain the tension in the stitch (UD-tight and UD-loose) or in the weft E-glass tows (UD-C). The sample length for fabric has been reduced to avoid the bench to bend and keep an equivalent surface of contact between the top PMMA plate and the sample (around two times  $70 \times 3.5 \text{ mm}^2$  for a tow test and around three times  $46.5 \times 3.5 \text{ mm}^2$  for a fabric test). Each test is repeated twice.

### Definition of the mechanical variables

Throughout the rest of this study, the fibrous sample cross-sections are considered rectangular and a uniform stress state is assumed along the thickness of the sample ( $z$ -direction).

The 6  $yz$  profiles recorded at each force level  $F$  allow the determination of the averaged thickness  $h$  and width  $w$  of the scanned sample. Large strain extensions are defined

$$\lambda_y = \frac{w}{w_0} \quad (1)$$

$$\lambda_z = \frac{h}{h_0} \quad (2)$$

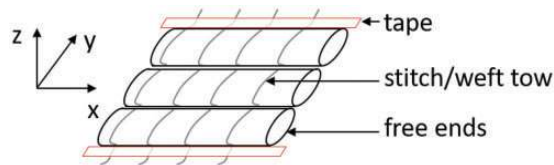


**Figure 2.** Boundary conditions applied for fabric tests: free ends and tape to maintain the stitch or weft tow tension.

where the initial width ( $w_0$ ) and thickness ( $h_0$ ) are measured for an initial force of 2N for both fabric and tow samples.

The Cauchy stress component in the transverse direction  $\sigma_z$  is defined as

$$\sigma_z = \frac{F}{wl} \quad (3)$$

where  $l$  is the length of the fibrous sample that is assumed constant during the compaction test due to fiber inextensibility.<sup>18,27</sup> Throughout the rest of the study, the Cauchy compressive stress  $\sigma_z$  is considered and plotted as positive. Figure 3 shows how the experimental results are analyzed using the mechanical variables defined hereinbefore.

### Experimental results and analysis

With the mechanical variables defined in the previous section, the experimental data obtained are first analyzed for carbon and E-glass tows and then for carbon and E-glass quasi-UDs. Although the experimental data were recorded over 6  $x$ -positions, the presence of stitch (UD-tight and UD-loose) or weft E-glass tows (UD-C) can lead to inaccurate width detection at 1 or 2  $x$ -positions. Therefore, in the following, it is indicated that the width and thickness evolutions are averaged over at least 4  $x$ -positions.

#### Carbon and E-glass tows: repeatability

Three carbon tows have been subjected to transverse compaction with the developed setup and the width and thickness evolutions have been averaged over at least 4  $x$ -positions along the tows. The resulting transverse (Figure 4(a)) and lateral (Figure 4(b)) behaviors are repeatable and consistent: for a given transverse

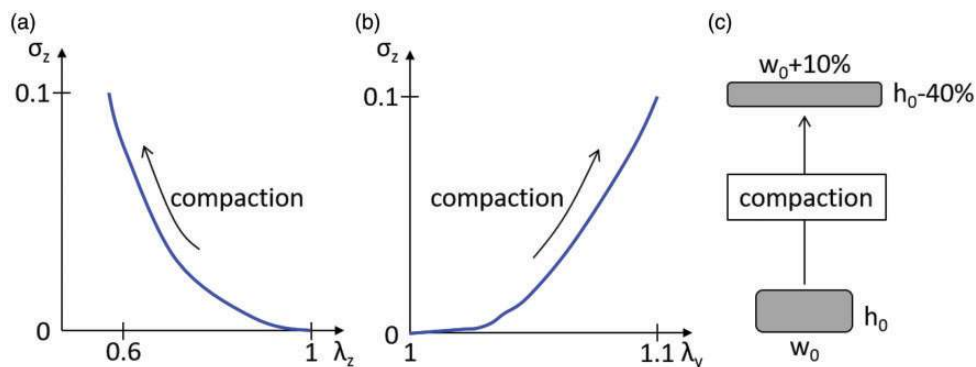


**Figure 3.** Typical stress-extension response during dry compaction: (a) evolution of the sample thickness extension ( $\lambda_z$ ), (b) evolution of the sample width extension ( $\lambda_y$ ), and (c) visualization of the corresponding sample cross-section.

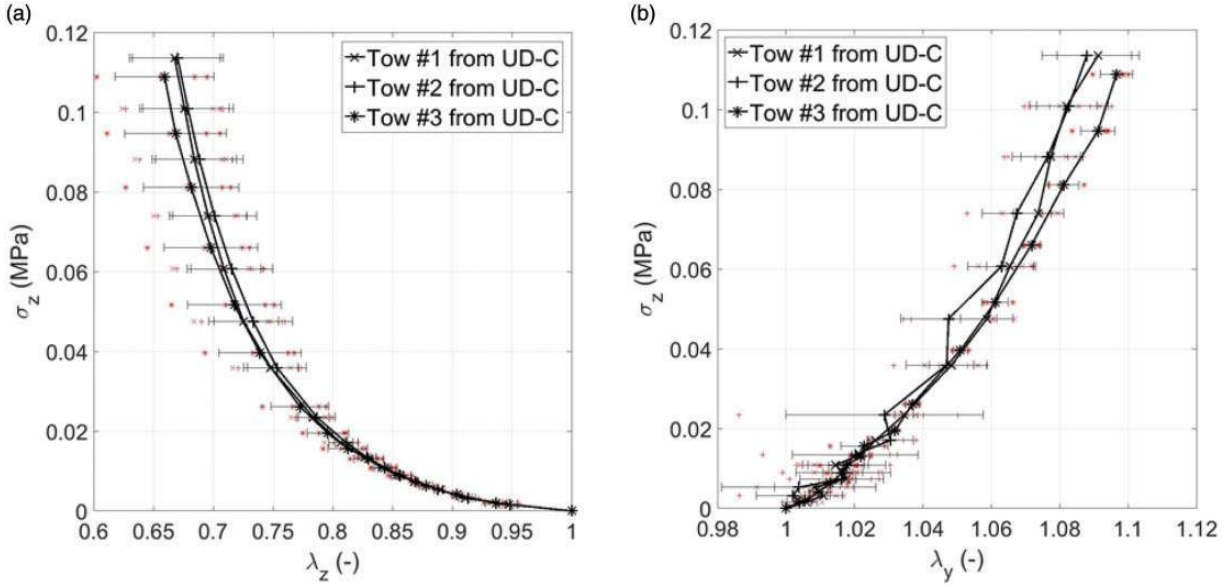


**Figure 4.** Compaction of carbon tow (extracted from UD-C): stress versus transverse (a) and lateral (b) strain extensions. Red points represent the raw data recorded along the longitudinal x-axis of the tow. UD-C: carbon quasi-unidirectional.

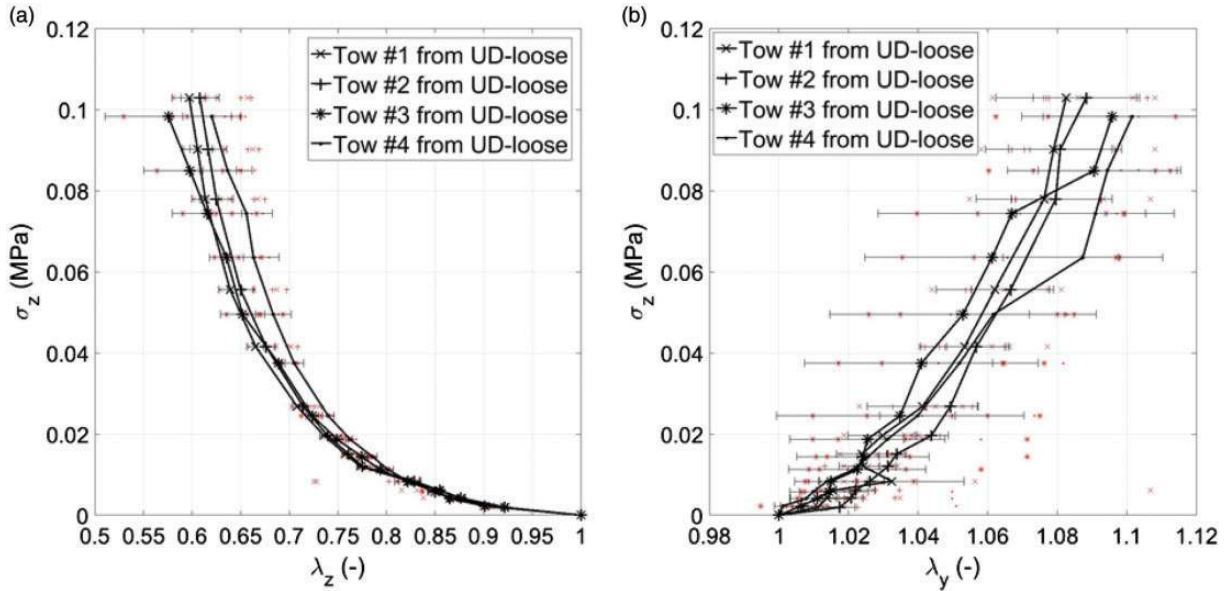


**Figure 5.** Compaction of E-glass tow (extracted from UD-loose): stress versus transverse (a) and lateral (b) strain extensions. Red points represent the raw data recorded along the longitudinal x-axis of the tow.

stress  $\sigma_z$  of 0.1 MPa, the carbon tow thickness reduces by  $37 \pm 3\%$  whereas width increases by  $8.5 \pm 1\%$ . Additionally, four E-glass tows extracted from UD-loose have been subjected to transverse compaction. Again, the resulting transverse (Figure 5(a)) and lateral (Figure 5(b)) behaviors are consistent: E-glass tows widen when subjected to transverse compaction (for  $\sigma_z$ , the thickness reduces by  $40 \pm 5\%$  whereas width

increases by  $9 \pm 3\%$ ). E-glass results are less repeatable than the carbon ones: it could be explained by the fact that an E-glass tow results from the assembly of two sub-tows whereas a carbon tow is made from a single tow. The constitutive element (i.e. tow) of carbon quasi-UD proves to be therefore more mechanically stable than the constitutive element of E-glass quasi-UD NCFs.

The behaviors of both the carbon and E-glass constitutive tows are averaged from now on in the following sections for clarity.

### Carbon quasi-UD: stiffening of the transverse behavior

Two samples of carbon quasi-UD have been subjected to compaction and both the transverse and the lateral evolutions (averaged over at least 4  $x$ -positions) are repeatable (Figure 6). The transverse behavior of the quasi-UDs is significantly stiffer than the one of the constitutive carbon tows (Figure 6(a)). Indeed, single tows, that are laterally free, significantly widen during compaction ( $8.5 \pm 1\%$  at 0.1 MPa) whereas tows inside the quasi-UDs, that are partially laterally confined, (the width of the quasi-UD increase only by  $2 \pm 0.8\%$  at 0.1 MPa, Figure 6(b)) densify. This densification of the quasi-UD, mainly due to the presence of the weft E-glass tows that confine laterally the carbon constitutive tows, induces a stiffening of the transverse behavior. Table 3 highlights sample cross-sections evolution while subjected to transverse compaction. It confirms that the fabric UD-C densify more than its respective carbon tow. The reader should refer to Dharmalingam et al.<sup>26</sup> for details concerning densification (compressibility) and flattening (incompressibility).

### E-glass quasi-UDs: influence of the stitch

The UD-loose transverse behavior (Figure 7(a)) is similar to the transverse behavior of its constitutive E-glass

tows whereas the UD-loose lateral extension remains lower than the lateral extension of its constitutive E-glass tows (Figure 7(b)). The UD-loose lateral evolution, difficult to capture due to the weft backing E-glass layer oriented at  $\pm 80^\circ$ , might be lower than the single tow lateral evolution due to side effects. Actually, no transverse stiffening of the UD-loose (compared to tows extracted from UD-loose) is recorded during the compaction: therefore, the E-glass tows inside the UD-loose are expected to widen. Indeed, the loose stitch allows tows widening within the inter-tow channels during the compaction, as highlighted in Figure 8(a) where inter-tows channels are hard to distinguish.

The transverse behavior of the UD-tight (Figure 7(a)) is significantly stiffer compared to the transverse

**Table 3.** Evolution of the tow and fabric cross-sections while subjected to transverse compaction.

	$\frac{h_f w_f}{h_0 w_0}$
Tows from UD-C	0.74
UD-C	0.71
Tows from UD-loose	0.66
UD-loose	0.63
Tows from UD-tight	0.79
UD-tight	0.74

The  $h_f$  and  $w_f$  are, respectively, the final thickness and width ( $\sigma_f = 0.1 \text{ MPa}$ ) and  $h_0$ ,  $w_0$  the initial thickness and width ( $\sigma_0 = 0 \text{ MPa}$ ).

**UD:** unidirectional; **UD-C:** carbon quasi-unidirectional.

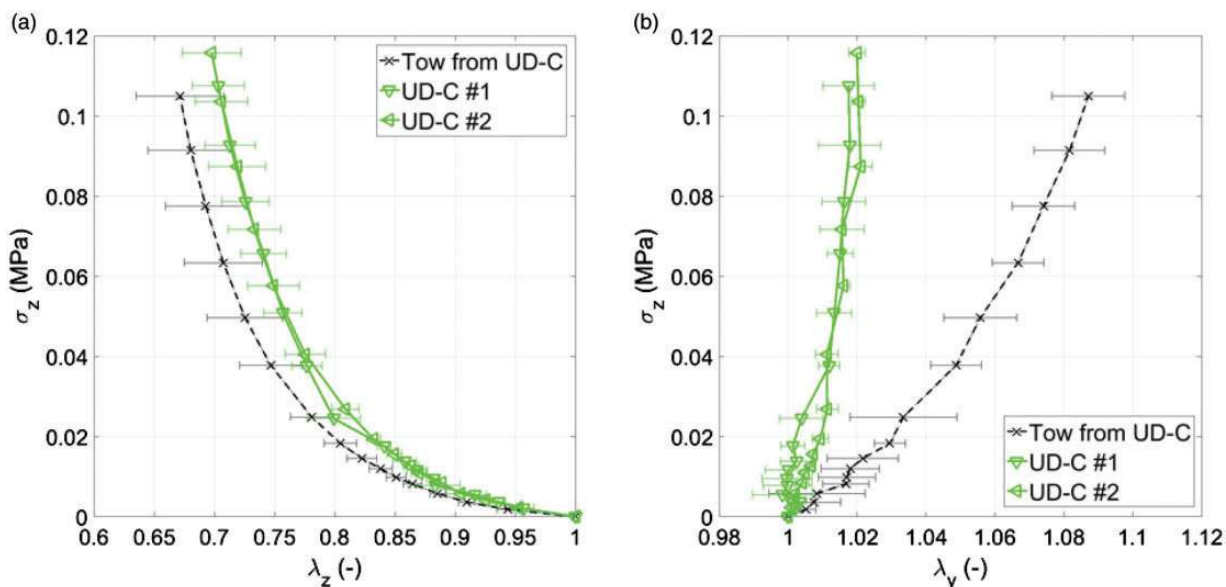


**Figure 6.** Compaction of UD-C (in green) and its corresponding constitutive tows (in black): stress versus transverse (a) and lateral (b) strain extensions. (For interpretation of the references to color in this figure legend, the reader is referred to the web version of this article.) UD-C: carbon quasi-unidirectional.

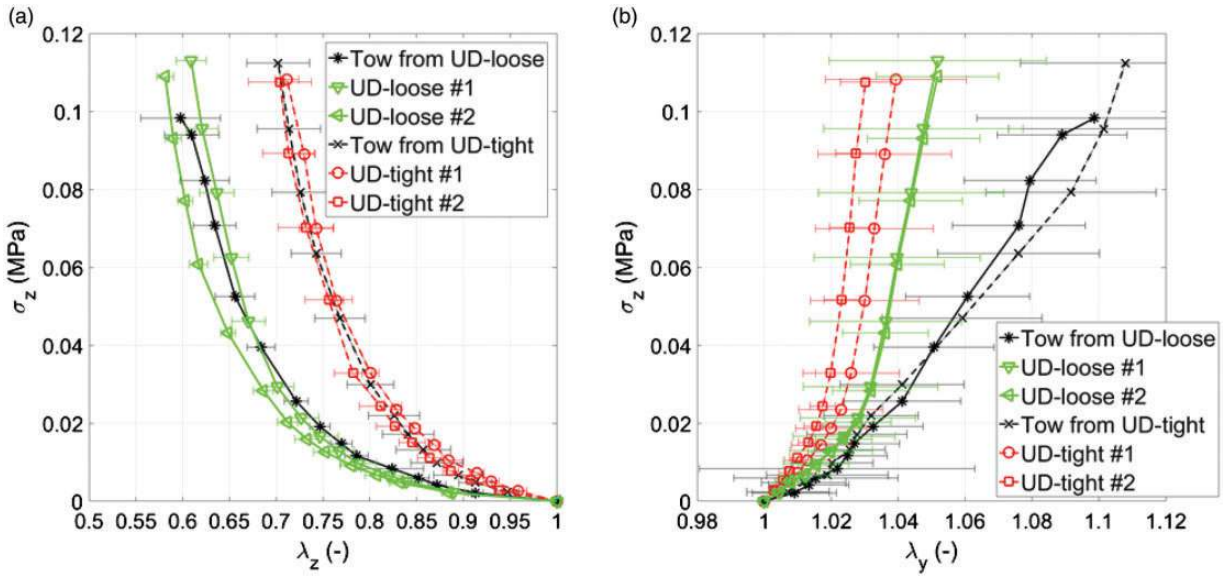


**Figure 7.** Compaction of UD-loose (in green) and UD-tight (in red) and their corresponding constitutive tows (in black): stress versus transverse (a) and lateral (b) strain extensions. (For interpretation of the references to color in this figure legend, the reader is referred to the web version of this article.)  
UD: unidirectional.

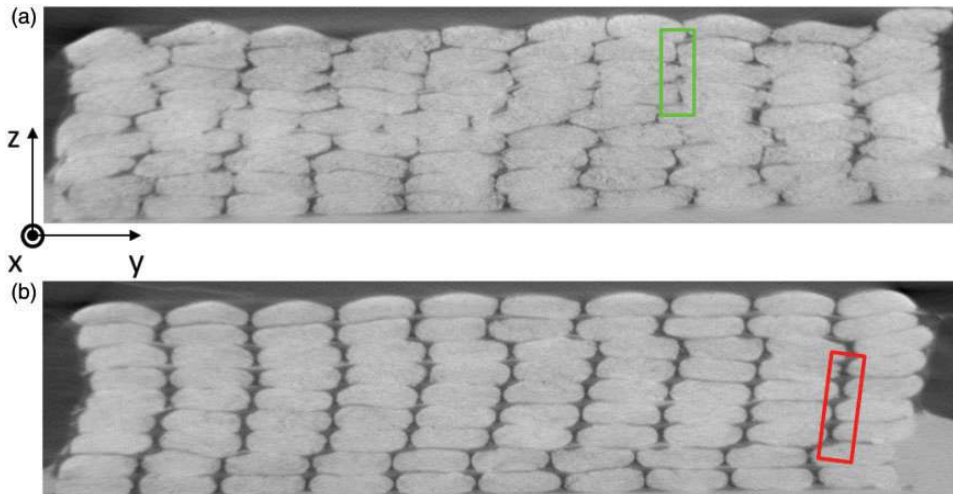


**Figure 8.** Microstructure recorded with X-ray Computed Tomography scan under vacuum (0.094 MPa, see Hemmer et al.<sup>28</sup> for more details): (a) UD-loose with small inter-tow channels (highlighted in green) and (b) UD-tight with large inter-tow channels (highlighted in red). (For interpretation of the references to color in this figure legend, the reader is referred to the web version of this article.)

behavior of the UD-loose whereas the total lateral extension of the UD-tight is slightly lower than the lateral extension of the UD-loose. A transverse stiffening (compared to the constitutive tows UD-loose) is recorded during the compaction: therefore the E-glass tows inside the UD-tight densify rather than widen, as highlighted in Figure 8(b) where the inter-tows channels remain large. The stitch seems tight enough to partially confine laterally the tows inside the UD-tight. Moreover,

the densification difference between tows extracted from UD-tight and UD-tight is larger than the one between tows extracted from UD-loose and UD-loose (Table 3).

Last experiments have been conducted on E-glass tows extracted from UD-tight. Keeping in mind that the tows, which constitute UD-tight and UD-loose are the same, the transverse behavior of tows extracted from UD-tight is significantly stiffer than the tows extracted from UD-loose (Figure 7(a)) even if their



lateral behavior can be considered as similar (Figure 7(b)). The stitching step appears to modify intrinsically the tows (for instance when the sewing needles hit the lateral tow edges): the initial tow cross-sections are indeed significantly different for E-glass tows extracted from UD-tight and UD-loose (Table 4). The stitching step influences thus the mechanical behavior of the two types of tows when subjected to transverse compaction.

### Experimental conclusions

The transverse and lateral mechanical behaviors of tows and quasi-UDs have been investigated. The studied carbon and E-glass tows exhibit a significant widening under transverse compaction when extracted from their corresponding quasi-UDs. These experimental results are in good agreement with the one obtained on single tows.<sup>26</sup> Nonetheless, the stitching process seems to modify intrinsically the E-glass tows and thus their corresponding transverse behavior.

Finally, the lateral confinement of tows that are inside a quasi-UD seems to depend on the stitch or the weft tow tension. This confinement induces a densification of the tows, leading thus to a stiffening of the corresponding quasi-UD transverse behavior.

### A simple 2D constitutive equation for tow cross-section

Accounting for the previous experimental results, the response of single tows during transverse compaction is revealed non-linear and highly compressible. Moreover, the influence of the lateral confinement on the transverse behavior has also been highlighted. In order to reproduce this response of the tow cross-section, a simple continuum mechanical approach is proposed in the present section. In the following, the material is considered homogeneous and transversally isotropic with respect to the fiber direction.

#### Isotropic large strain compressible elasticity

Recently, some authors propose to consider large strain hyperelastic models as the basis for the development of

**Table 4.** Initial thickness ( $h_0$ ) and width ( $w_0$ ) of E-glass tows extracted from UD-tight and UD-loose.

	$h_0$ (mm)	$w_0$ (mm)
Tows from UD-tight	$1.138 \pm 0.064$	$3.594 \pm 0.065$
Tows from UD-loose	$1.289 \pm 0.194$	$4.178 \pm 0.309$

UD: unidirectional.

constitutive equations for tows during compaction.<sup>29</sup> Such models, initially developed for elastomers that are considered incompressible,<sup>30</sup> have been extended in various manner to consider the compressible response of elastomers in specific conditions, of foam rubbers, or of biological tissues.<sup>20,31</sup>

Here, a one-term Ogden-Hill constitutive equation is considered and defined by the following strain energy density, defined per unit of undeformed volume

$$W = \frac{2\mu}{\alpha^2} \left( \lambda_1^\alpha + \lambda_2^\alpha + \lambda_3^\alpha - 3 + \frac{1}{\beta} (J^{-\alpha\beta} - 1) \right) \quad (4)$$

where  $(\lambda_i)_{i=1,2,3}$  are the principal stretch ratios and  $J = \lambda_1\lambda_2\lambda_3$  is the Jacobian of deformation, which reflects the change in volume induced by the deformation. This model depends on three material parameters (positive scalars):

- $\mu$  is the shear modulus,
- $\alpha$  induces the non-linear response as proposed by Seth,<sup>32</sup>
- and  $\beta$  drives the compressible response.

The first term in the right-hand side of equation (4) was proposed by Ogden,<sup>33</sup> and the second one by Hill<sup>34</sup> inspired by the proposal of Blatz and Ko for foam rubbers.<sup>35</sup> For a more general formulation of the Ogden-Hill approach, the reader can refer to the work of Jemio and Turteltaub.<sup>36</sup> Finally, it is to be noted that the material parameter  $\mu$  is defined differently than in the above-mentioned papers: it corresponds to the definition of the ‘‘Hyperfoam’’ model implemented in the commercial software Abaqus and considered for example by Berezvai and Kossa.<sup>37</sup>

Once the strain energy density function defined in terms of the principal stretch ratios, the principal true (Cauchy) stresses  $(\sigma_i)_{i=1,2,3}$  can be derived<sup>38</sup>

$$\sigma_i = \frac{1}{J} \lambda_i \frac{\partial W}{\partial \lambda_i} \quad \text{for } i = 1, 2, 3 \quad (5)$$

After basic algebraic manipulations, these principal stress reduces to

$$\sigma_i = \frac{2\mu}{\alpha} \frac{1}{J} (\lambda_i^\alpha - J^{-\alpha\beta}) \quad (6)$$

#### Inextensibility of fibers

The first method to consider the high stiffness in the fibers direction would consist in adopting a transversely isotropic hyperelastic constitutive equation.<sup>39</sup>

The aim of the present derivation is to propose a simple model to reproduce the response of the tow

cross-section. Thus, it is possible to derive the corresponding 2D constitutive equation in a simpler manner.  $x$  is the fiber direction as depicted in Figure 9(a).

First, only deformation processes that maintain this direction unchanged are considered:  $x$  is a principal direction of the deformation and the corresponding stretch ratio is denoted  $\lambda_x$ . Second, the fibers are considered inextensible. These two assumptions summarize in the following internal constraint

$$\lambda_x = 1 \quad (7)$$

Nevertheless, such a constraint impacts the derivation of the stresses. Indeed, it exist an additional stress  $\gamma$  in the  $x$ -direction such that equation (5) becomes

$$\sigma_x = \frac{1}{J} \lambda_x \frac{\partial W}{\partial \lambda_x} + \gamma \quad (8)$$

This additional stress does not depend on the material but on the given mechanical problem. From a theoretical point of view, it plays the same role as the hydrostatic pressure for incompressible materials; for more details, the interested reader can refer to the work of Truesdell and Noll<sup>40</sup> (p. 69).

Finally, denoting  $\lambda_y$  and  $\lambda_z$  the principal stretch ratios in the tow cross-section, and considering equations (6) to (8), the principal true stresses are

$$\sigma_x = \frac{2\mu}{\alpha} ((\lambda_y \lambda_z)^{-1} - (\lambda_y \lambda_z)^{-\alpha\beta-1}) + \gamma \quad (9)$$

$$\sigma_y = \frac{2\mu}{\alpha} (\lambda_y^{\alpha-1} \lambda_z^{-1} - (\lambda_y \lambda_z)^{-\alpha\beta-1}) \quad (10)$$

and,

$$\sigma_z = \frac{2\mu}{\alpha} (\lambda_y^{-1} \lambda_z^{\alpha-1} - (\lambda_y \lambda_z)^{-\alpha\beta-1}) \quad (11)$$

In the following, the experimental data recorded on tows will be used to determine the model parameters. Therefore, it will be assumed that the mechanical response of the tow is homogeneous along the fibers ( $x$ -direction). Moreover, as shown in Figure 9(b), the experimental loading directions always correspond to the principal directions of deformation and the friction is assumed negligible between the fibrous sample and the experimental device (no shear). Indeed, only the set of equations (10) and (11) will be considered and referred to as the ‘‘2D constitutive model’’ for sake of simplicity.

### Two special cases: laterally free and confined boundary conditions

Two set of boundary conditions are now examined: laterally free and confined tow. They are depicted in Figure 10(a) and (b), respectively, where tow cross-sections are still assumed rectangular.

- In the former case, the tow is free to expand in the  $y$ -direction such that  $\sigma_y = 0$ . Solving this equation in terms of  $\lambda_y$  leads to the following transverse true stress

$$\sigma_z^{\text{free}} = \frac{2\mu}{\alpha} \left( \lambda_z^{\frac{\alpha\beta+\alpha-1}{1+\beta}} - \lambda_z^{\frac{-\alpha\beta-1}{1+\beta}} \right) \quad (12)$$

Note that the corresponding lateral stretch ratio is

$$\lambda_y = \lambda_z^{\frac{-\beta}{1+\beta}} \quad (13)$$

- In the latter case, the tow cannot expand laterally, such that  $\lambda_y = 1$ . Then, the corresponding transverse true stress is

$$\sigma_z^{\text{conf}} = \frac{2\mu}{\alpha} (\lambda_z^{\alpha-1} - \lambda_z^{-\alpha\beta-1}) \quad (14)$$

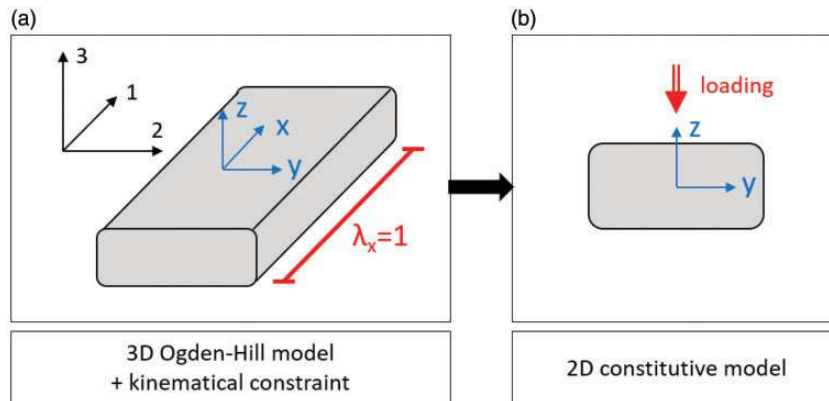
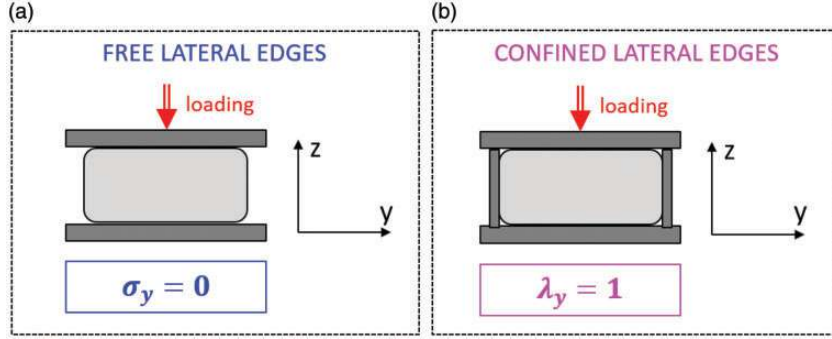


Figure 9 Representation of the 3D (a) and resulting 2D (b) mechanical problem.



**Figure 10.** Cross-section of a single tow subjected to transverse compaction: (a) laterally free boundary condition and (b) laterally confined boundary condition.

## Modeling results and analysis

The 2D constitutive model is used here to propose a novel investigation of the lateral confinement influence on the transverse mechanical behavior of tows subjected to compaction. First, the material parameters are identified by fitting the laterally free analytical solution (equation (12)) with the experimental data recorded on tows. Then, the influence of the boundary conditions on the transverse mechanical behavior is investigated by keeping the same material parameters. Finally, still keeping the same material parameters, the laterally confined analytical predicted solution (equation (14)) is compared to the experimental data recorded on quasi-UDs, where tows are partially laterally confined.

### Identification: material parameters and sensitivity

The material parameters  $\mu$ ,  $\alpha$ ,  $\beta$  have been obtained with the following fitting procedure:

- $\beta$  is computed using equation (13). As its value varies during the transverse compaction experiments, its maximal value has been selected to best fit the large lateral deformations undergone by tows.
- Once  $\beta$  selected, a constrained non-linear fit is carried out using equation (12), where  $\mu > 0$  and  $\mu * \alpha > 0$  (to ensure stability condition<sup>30</sup>).

The values obtained for carbon and E-glass tows are reported in Table 5. The model curve obtained with the carbon material parameters fits well with the experimental transverse behavior (Figure 11(a)) whereas the lateral behavior fitting appears improvable (Figure 11(b)). The influence of the selected value of  $\beta$  is thus investigated and confirms that the highest value of  $\beta$  ensures a better fit with the large lateral deformations (Figure 11(b)). The obtained material parameters (Table 5) remain unchanged for the rest of the study.

**Table 5.** Materials parameters of the constitutive model for carbon and E-glass tows.

	Carbon tows ( $j = C$ )	E-glass tows ( $j = E$ )
$\mu_j$	0.05 (MPa)	0.04 (MPa)
$\alpha_j$	43 (-)	36 (-)
$\beta_j$	0.26 (-)	0.22 (-)

### Prediction: boundary conditions influence

Figure 12 presents the experimental results obtained during the compaction of carbon tows, the fitted laterally free constitutive model (equation (12)) and the predicted laterally confined constitutive model (obtained with equation (14) and the carbon material parameters in Table 5). As expected, the confined tow width remains constant during the compaction ( $\lambda_y = 1$  in Figure 12(b)). This lateral confinement induces a stiffening of the transverse behavior (Figure 12(a)) the modeled confined tow cannot widen during the compaction and thus densifies. This densification has been previously observed in the experimental behavior of quasi-UDs. A comparison between the predicted confined tow and the experimental quasi-UDs mechanical behaviors is thus proposed in the following section.

### Comparison: laterally confined modeled tows behavior and experimental quasi-UDs behavior

Regarding the carbon material behavior during compaction (Figure 13(a)), the UD-C transverse evolution is stiffer than the one of laterally free carbon tows (experimental) while remaining less stiff than the transverse behavior of a fully confined carbon tow (predicted with the constitutive model). Moreover, the fabric width extension remains lower than the one of laterally free tows (Figure 13(b)). These results are in good agreement with the proposed experimental conclusions:

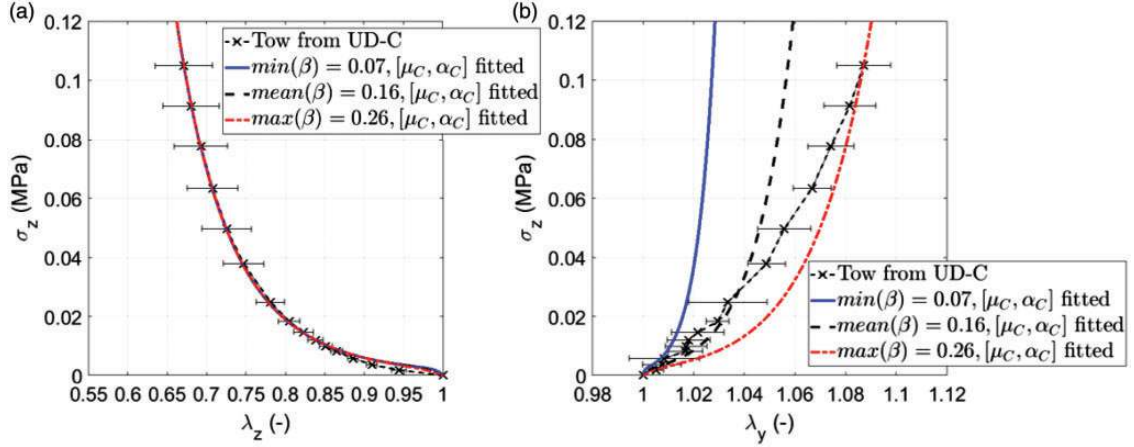


**Figure 11.** Comparison between the experimental and the modeled carbon (laterally free) tow behavior and visualization of  $\beta$  selection impact: stress versus transverse (a) and lateral (b) strain extensions. UD: unidirectional.

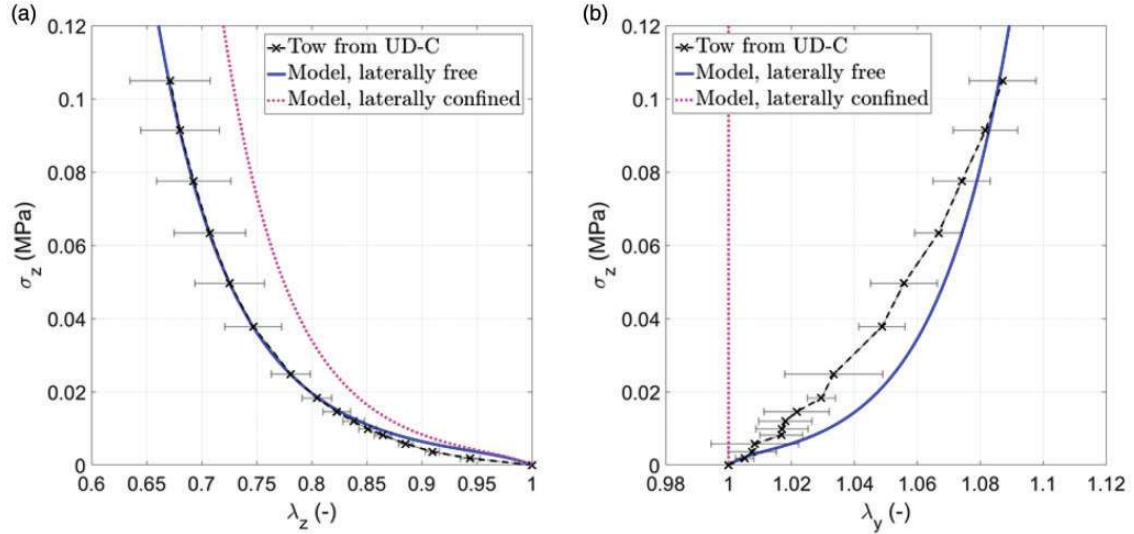


**Figure 12.** Experimental data recorded on carbon tows (in black) and the corresponding laterally free (in blue) and laterally confined (in pink) modeled behaviors: stress versus transverse (a) and lateral (b) strain extensions. (For interpretation of the references to color in this figure legend, the reader is referred to the web version of this article.) UD-C: carbon quasi-unidirectional.

the carbon tows located inside the UD-C are partially laterally confined, leading thus to a slight transverse stiffening compared to a laterally free tow. This stiffening remains lower than the one of a fully confined tow (modeled).

Regarding the E-glass material (Figure 14), UD-tight transverse behavior is stiffer than the one predicted for a laterally confined tow. This result might be interpreted as follows. The tows extracted from UD-tight are themselves stiffer than tows extracted from UD-loose because they have been intrinsically

modified by the stitching process. The comparison proposed here between UD-loose and UD-tight is actually the comparison of two different constitutive materials. Therefore, the methodology, which consists of keeping material parameters to compare laterally free tows and quasi-UDs is not applicable for the studied E-glass material. Additionally, it should be noticed that assuming a rectangular cross-section as well as a uniform stress state along the  $z$ -direction might explain to some extent the difference between the experimental and modeled mechanical behaviors.

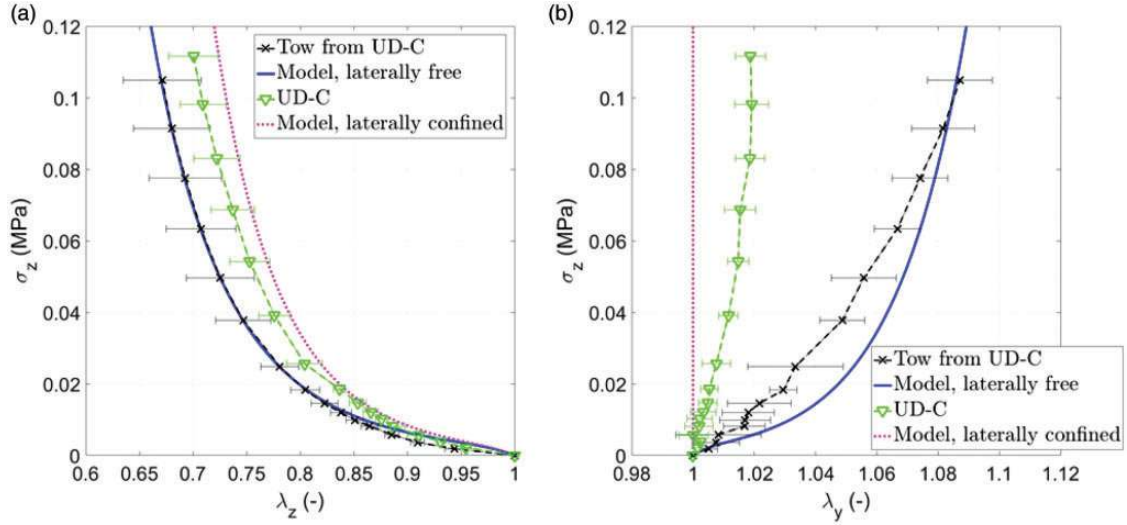


**Figure 13.** Comparison between carbon quasi-UD experimental behavior (in green) and predicted confined tow behavior (in pink): stress versus transverse (a) and lateral (b) strain extensions. (For interpretation of the references to color in this figure legend, the reader is referred to the web version of this article.)  
UD-C: carbon quasi-unidirectional.

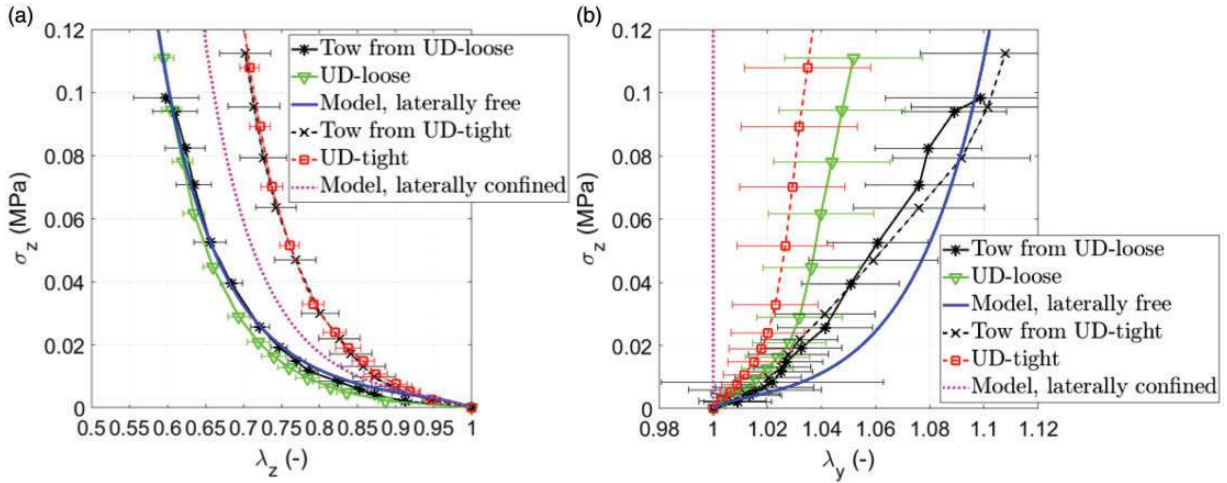


**Figure 14.** Comparison between E-glass quasi-UDs (UD-loose in green and UD-tight in red) experimental behaviors and predicted confined tow behavior (in pink): stress versus transverse (a) and lateral (b) strain extensions. (For interpretation of the references to color in this figure legend, the reader is referred to the web version of this article.)  
UD: unidirectional.

## Conclusion

Novel experiments have been conducted to quantify the width and thickness evolutions experienced by quasi-UDs and their constitutive tows during through-thickness compaction. The studied carbon and E-glass tows exhibit a significant widening when laterally free i.e. when extracted from their corresponding quasi-UDs. However, the lateral confinement of tows that remain inside their corresponding quasi-UD depends on the

stitch or weft tow tension. This partial confinement induces a densification of the tows leading to a stiffening of the corresponding quasi-UD transverse behavior.

A 2D constitutive model has been built from the hyperelastic Ogden-Hill 3D model and found to be appropriate to reproduce the lateral and transverse non linear elastic behaviors of tows during compaction. A novel boundary condition has been proposed in this work to predict the mechanical behavior of a given tow that is fully confined in width direction during

compaction. This predicted confined behavior has been compared to the experimental behavior of quasi-UDs, where a lateral tow confinement is expected due to the stitch or the weft tow tension. When the constitutive tows are not intrinsically modified by the stitching or the sewing process, the corresponding quasi-UD mechanical behavior fits well between the one of laterally free tows (measured) and of fully laterally confined tows (predicted).

The presented approach consists of characterizing finely the lateral and transverse behaviors of constitutive tows and uses the proposed constitutive model to predict a possible range for quasi-UDs transverse mechanical behavior. This methodology might help textile designers in adjusting their process parameters as, for instance, the stitch tension. Additionally, knowing the constitutive tow behavior and the quasi-UD transverse behavior could lead to a novel indicator of the porous mesostructural organization (inter-tow channels size) whose knowledge is essential for permeability and filling time estimations.<sup>13,15</sup> Finally, an isotropic transverse strain energy, weighted with a large stiffness parameter in the fiber direction (as done for biological soft tissues<sup>41</sup>), can be added to the 3D Ogden-Hill model to account for fiber quasi-inextensibility. The obtained 3D model could be integrated in a computational framework as done to account for the tows widening occurring during longitudinal compaction.<sup>20</sup>

Future work will focus on releasing the assumption of a rectangular cross-section, as a non-uniform stress state inside the tow might influence the overall fabric compaction behavior.<sup>42</sup> Once done, it would allow to investigate the influence of the tow twist (that induces rounder cross-sections) on the compaction behavior.


### Declaration of Conflicting Interests

The author(s) declared no potential conflicts of interest with respect to the research, authorship, and/or publication of this article.

### Funding

The author(s) received no financial support for the research, authorship, and/or publication of this article.

### ORCID iD

Julie Hemmer  <https://orcid.org/0000-0002-8487-667X>

### References

1. Kruckenberg T, Ye L and Paton R. Static and vibration compaction and microstructure analysis on plain-woven textile fabrics. *Compos Part A Appl Sci Manuf* 2008; 39: 488–502.
2. Simacek P and Karbhari VM. Notes on the modeling of preform compaction: I-micromechanics at the fiber bundle level. *J Reinf Plast Compos* 1996; 15: 86–122.
3. Bickerton S, Buntain M and Somashekar A. The viscoelastic compression behavior of liquid composite molding preforms. *Compos Part A Appl Sci Manuf* 2003; 34: 431–444.
4. Comas-Cardona S, Grogneq PL, Binetruy C, et al. Unidirectional compression of fibre reinforcements. Part 1: a non-linear elastic-plastic behaviour. *Compos Sci Technol* 2007; 67: 507–514.
5. Aranda S, Klunker F and Ziegmann G. Compaction response of fibre reinforcements depending on processing temperature. In: *17th International conference on composite materials (ICCM 17)*, Edinburgh, July 2009.
6. Vallons K, Adolphs G, Lucas P, et al. The influence of the stitching pattern on the internal geometry, quasi-static and fatigue mechanical properties of glass fibre non-crimp fabric composites. *Compos Part A Appl Sci Manuf* 2014; 56: 272–279.
7. Yenilmez B and Sozer EM. Compaction of e-glass fabric preforms in the vacuum infusion process, a: characterization experiments. *Compos Part A Appl Sci Manuf* 2009; 40: 499–510.
8. van Wyk CM. 20–Note on the compressibility of wool. *J Text Inst Trans* 1946; 37: T285–T292.
9. Robitaille F and Gauvin R. Compaction of textile reinforcements for composites manufacturing. *Polym Compos* 1999; 20: 48–61.
10. Gutowski TG, Morigaki T and Cai Z. The consolidation of laminate composites. *J Compos Mater* 1987; 21: 172–188.
11. Chen B and Chou TW. Compaction of woven-fabric preforms in liquid composite molding processes: single-layer deformation. *Compos Sci Technol* 1999; 59: 1519–1526.
12. Syerko E, Binetruy C, Comas-Cardona S, et al. A numerical approach to design dual-scale porosity composite reinforcements with enhanced permeability. *Mater Des* 2017; 131: 307–322.
13. Caglar B, Orgéas L, Rolland du Roscoat S, et al. Permeability of textile fabrics with spherical inclusions. *Compos Part A Appl Sci Manuf* 2017; 99: 1–14.
14. Salvatori D, Caglar B, Teixidó H, et al. Permeability and capillary effects in a channel-wise non-crimp fabric. *Compos Part A Appl Sci Manuf* 2018; 108: 41–52.
15. Endruweit A, Zeng X, Matveev M, et al. Effect of yarn cross-sectional shape on resin flow through inter-yarn gaps in textile reinforcements. *Compos Part A Appl Sci Manuf* 2018; 104: 139–150.
16. Ghayoor H, Marsden CC, Hoa SV, et al. Numerical analysis of resin-rich areas and their effects on failure initiation of composites. *Compos Part A Appl Sci Manuf* 2019; 117: 125–133.
17. Nguyen Q, Vidal-Sallé E, Boisse P, et al. Mesoscopic scale analyses of textile composite reinforcement compaction. *Compos Part B Eng* 2013; 44: 231–241.
18. Swery E, Allen T and Kelly P. Predicting compaction-induced deformations of meso-scale textile models efficiently. *J Compos Mater* 2016; 51.
19. Naouar N, Vidal-Sallé E, Schneider J, et al. Meso-scale fe analyses of textile composite reinforcement deformation based on x-ray computed tomography. *Compos Struct* 2014; 116: 165–176.

20. Wang D, Naouar N, Vidal-Salle E, et al. Longitudinal compression and poisson ratio of fiber yarns in meso-scale finite element modeling of composite reinforcements. *Compos Part B Eng* 2018; 141: 9–19.
21. Naouar N, Vidal-Salle E, Schneider J, et al. 3D composite reinforcement meso f.e. analyses based on x-ray computed tomography. *Compos Struct* 2015; 132: 1094–1104.
22. Potluri P, Thammandra V and Ramgulam R. Modelling tow compression in textile preforms during composites processing. In: *ASME 2004 International Mechanical Engineering Congress and Exposition*, American Society of Mechanical Engineers, pp.415–419.
23. Harwood R, Grishanov S, Lomov S, et al. Modelling of two-component yarns part I: the compressibility of yarns. *J Text Inst* 1997; 88: 373–384.
24. Zhou G, Sun X and Wang Y. Multi-chain digital element analysis in textile mechanics. *Compos Sci Technol* 2004; 64: 239–244.
25. Yousaf Z, Potluri P, Withers P, et al. Digital element simulation of aligned tows during compaction validated by computed tomography (ct). *Int J Solids Struct* 2018; 154: 78–87.
26. Dharmalingam AS, Hemmer J, Lectez AS, et al. Evolution of single carbon and glass fibrous tow cross-sections in dry and lubricated states during compaction perpendicular to the fibers. *Compos Part B Eng* 2018; 148: 235–242.
27. Vidal-Sallé E, Nguyen Q, Charmetant A, et al. Use of numerical simulation of woven reinforcement forming at mesoscale: influence of transverse compression on the global response. *Int J Mater Form* 2010; 3: 699–702.
28. Hemmer J, Burtin C, Comas-Cardona S, et al. Unloading during the infusion process: direct measurement of the dual-scale fibrous microstructure evolution with x-ray computed tomography. *Compos Part A Appl Sci Manuf* 2018; 115: 147–156.
29. Lectez AS, El Azzouzi K, Binetruy C, et al. Three-dimensional mechanical properties of dry carbon fiber tows subjected to cyclic compressive loading. *J Compos Mater* 2018; 52: 2661–2677.
30. Marckmann G and Verron E. Comparison of hyperelastic models for rubberlike materials. *Rubber Chem Technol* 2006; 79: 835–858.
31. Boyce MC and Arruda EM. Constitutive models of rubber elasticity: a review. *Rubber Chem Technol* 2000; 73: 504–523.
32. Seth B. Generalized strain measure with applications to physical problems. In: Reiner M and Abir D (eds) *Second order effects in elasticity, plasticity and fluid dynamics*. New York: McMillan, 1964, pp.162–172.
33. Ogden RW. Large deformation isotropic elasticity: on the correlation of theory and experiment for compressible rubberlike material. *Proc R Soc London Ser A* 1972; 328: 567–583.
34. Hill R. Aspects of invariance in solid mechanics. *Adv Appl Mech* 1978; 18: 1–75.
35. Blatz PJ and Ko WL. Application of finite elastic theory to the deformation of rubbery materials. *Trans Soc Rheol* 1962; 6: 223–252.
36. Jemiolo S and Turteltaub S. A parametric model for a class of foam-like isotropic hyperelastic materials. *J Appl Mech* 2000; 67: 248–254.
37. Berezvai S and Kossa A. Closed-form solution of the ogden–hill’s compressible hyperelastic model for ramp loading. *Mech Time Depend Mater* 2017; 21: 263–286.
38. Holzapfel GA. *Nonlinear solid mechanics: a continuum approach for engineering*. Chichester: Wiley & Sons Ltd, 2000.
39. Spencer AJM. *Continuum theory of the mechanics of fibre-reinforced composites*. Vol 282, Vienna: Springer, 1984.
40. Truesdell C and Noll W. *The non-linear field theories of mechanics*. Springer, 2004.
41. Velardi F, Fraternali F and Angelillo M. Anisotropic constitutive equations and experimental tensile behavior of brain tissue. *Biomech Model Mechanobiol* 2006; 5: 53–61.
42. Bancora S, Binetruy C, Advani S, et al. A new scalable methodology to predict permeability of deformed textiles under compression. In: *ICCM22 proceedings*, Melbourne, Australia.